Measurements of Cosmic Ray Mass Composition with the IceCube Neutrino Observatory

Matthias Plum[1,*] for the IceCube Collaboration

[1]South Dakota School of Mines and Technology, Rapid City, SD 57701 USA

Abstract. The IceCube Neutrino Observatory is a multi-component detector at the South Pole. Besides studying high-energy neutrinos, it is capable of measuring high-energy cosmic rays from PeV to EeV. This energy region is thought to cover the transition from galactic to extragalactic sources of cosmic rays. The observatory consists of the deep in-ice IceCube array, which measures the high-energy ($\geq$ 500 GeV) muonic component, and the IceTop surface array, which is sensitive to the electromagnetic and low-energy muonic part of an air shower. The primary energy and the mass composition can be measured simultaneously by applying statistical methods including modern machine-learning techniques to reconstruct cosmic ray air showers. In this contribution, we will discuss recent improvements to the reconstruction techniques, the mass composition sensitivity, and an outlook on future improved measurements with the full surface scintillator/radio array to mitigate snow accumulation and measure the air shower maximum X_{max} using imaging air-Cherenkov telescopes IceAct.

1 Introduction

High-energy cosmic rays are observed indirectly through the extensive air showers they initiate in the Earth's atmosphere. By measuring the electromagnetic and muonic shower components simultaneously, the mass and energy of the primary cosmic ray can be studied. However, the interpretation of such measurements in terms of the properties of the primary nucleus relies on detailed simulations of the air shower development.

2 IceCube and IceTop

IceCube [1] is a cubic-kilometer astroparticle detector installed in the ice at the geographic South Pole between depths of 1450 m and 2450 m, completed in 2010. The detector setup is shown in Figure 1 together with a schematic of the air shower detection capabilities of the surface and the in-ice component. It consists of 86 detector strings instrumented with 60 digital optical modules (DOMs). The deep in-ice detector IceCube, designed for high-energy neutrino astronomy, is complemented by the square-kilometer surface array IceTop [3], designed to measure the secondary particles from cosmic ray air showers. IceTop consists of 81 surface stations composed of two tanks separated by 10 m. Each tank is an ice-Cherenkov detector with two DOMs, one operating at low gain and the other at high gain, to maximize the dynamic range of the detector. The IceTop and the IceCube arrays can study astroparticle events independently or in coincidence. The IceTop tank signal is dominated by the electromagnetic component of incoming cosmic ray air showers, which allows a reconstruction of the primary energy and the geometry of the air showers. The in-ice array, on the other hand, can only measure the high-energy muon component of the air showers, which allows for the direct study of TeV-muon bundles. Together both detector arrays provide a unique environment for the study of the properties of primary cosmic rays over a wide energy range from PeV to EeV.

3 IceTop-IceCube Cosmic Ray Mass Composition

The combination of IceTop and IceCube events provides a good means to measure the primary mass composition. Using the tank signals, the core position and direction of the shower axis are reconstructed by fitting the signal times. A primary energy proxy is obtained by fitting the following function to the signal charges as a function of radial distance R to the shower axis:

$$S(R) = S_{125} \cdot \left(\frac{R}{125\,\mathrm{m}}\right)^{-\beta-\kappa\cdot\log_{10}\left(\frac{R}{125\,\mathrm{m}}\right)} \quad (1)$$

where $\kappa = 0.303$ as obtained from simulations (Sibyll2.1 [4]), and the free fit parameters β and S_{125} represent the slope of the function and the signal strength at a reference distance of 125 m respectively. An example of the air shower reconstruction in the spatial and time domain is shown in Figure 2. As snow accumulation above the tanks causes a fraction of the shower particles to be absorbed, the reconstruction modifies the expectations from Eq. 1 to account for the additional snow attenuation. S_{125} is highly correlated to the primary particle's energy as

*e-mail: matthias.plum@icecube.wisc.edu

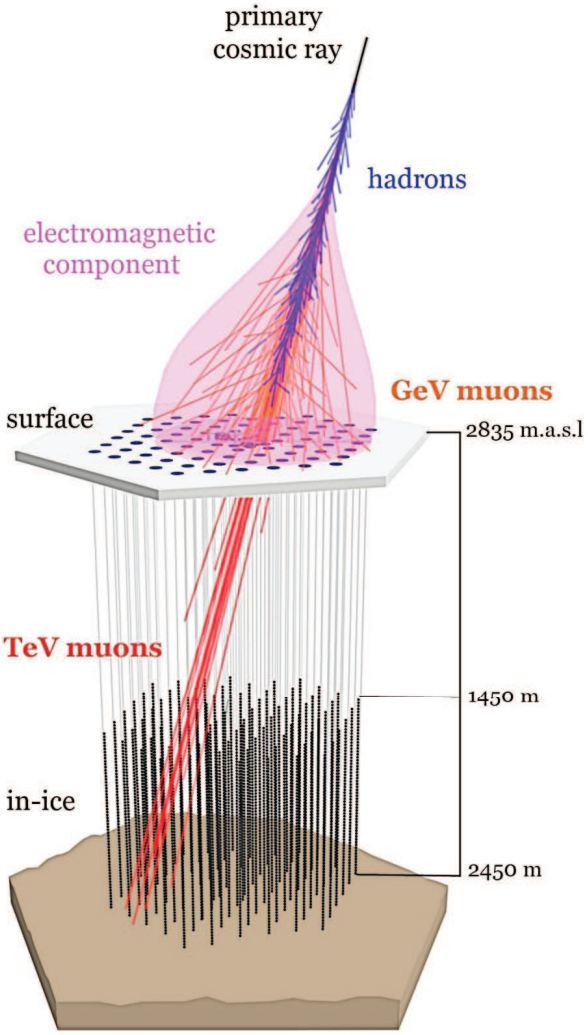

Figure 1: Air shower measurements of the IceCube Neutrino Observatory with the in-ice IceCube and surface IceTop array [2].

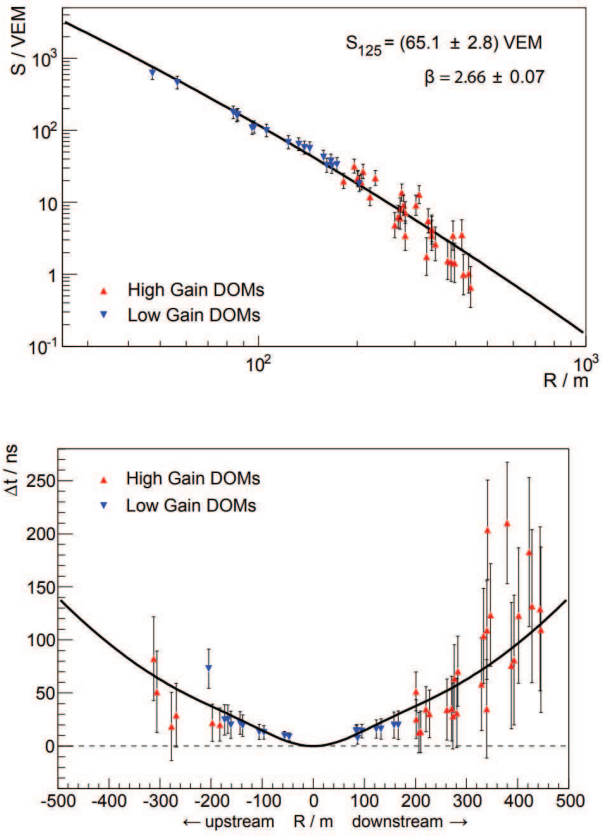

Figure 2: Example of the IceTop air shower reconstruction [3]. (Top) Lateral fit to signals from 25 triggered stations with a reconstructed shower size $S_{125} = (65.1 \pm 2.8)$ VEM. (Bottom) Time residuals with respect to a plane perpendicular to the shower direction. "Upstream" and "downstream" refer to tanks being hit before and after the shower core reaches the ground.

shown in Figure 3. The shower axis from IceTop reconstruction is used to determine the shower axis from the high-energy muon bundle in the in-ice IceCube detector. With this axis, the energy loss of the muon bundle can be measured as a function of slant depth. An example of the reconstructed energy deposit profile is shown in Figure 4. This energy deposit profile is evaluated at a reference slant depth of 1500 m. As shown in Figure 5, the energy loss at this depth is highly mass composition sensitive. As high-energy muons have a higher probability of losing larger energy clumps in stochastic processes, which produce spikes in the energy deposit profile. The number of those stochastic losses is counted as they increase the composition sensitivity of the analysis. Combining reconstructed detector observables from IceTop (S_{125}, zenith) and IceCube ($dE/dX_{1500\,m}$, number of high energy stochastic losses) using a dedicated Neural Network (NN) reconstruction, the energy and the mass composition of the primary cosmic ray are studied. The NN is trained to deliver an estimate for each event's energy and mass. While the

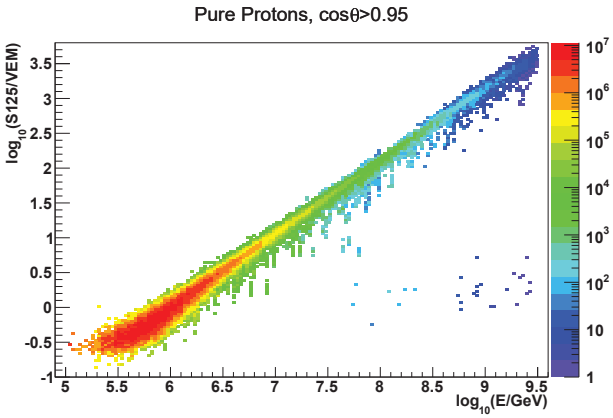

Figure 3: Correlation between S_{125} and primary energy in IceTop for proton simulations [5] using Sibyll2.1 [4].

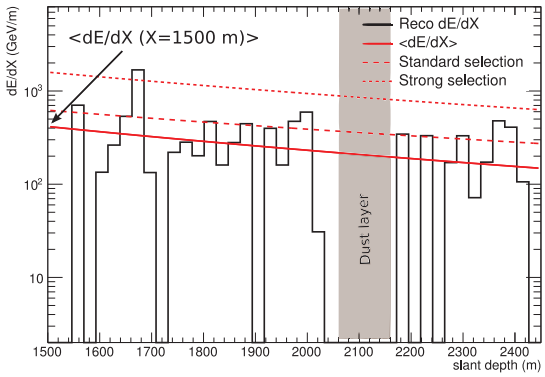

Figure 4: Energy loss reconstruction of an example air shower [5] event, where the solid red line demonstrates the average energy loss fit, the dashed red and dotted red lines indicate the standard and strong stochastics selection, respectively. The gray band is the approximate location of the dust layer for the slant depth of this particular event.

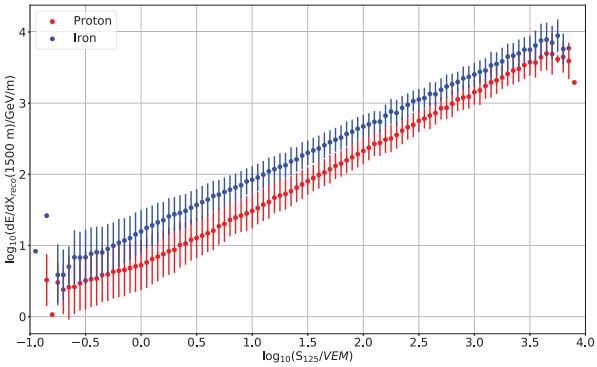

Figure 5: The composition sensitivity of the reconstructed energy loss parameter (dE/dX) at 1500 m slant depth for a given S_{125} for H and Fe simulation [5] using Sibyll2.1 [4]. The error bars indicate the 1-sigma width of the (dE/dX) distribution for a given S_{125}.

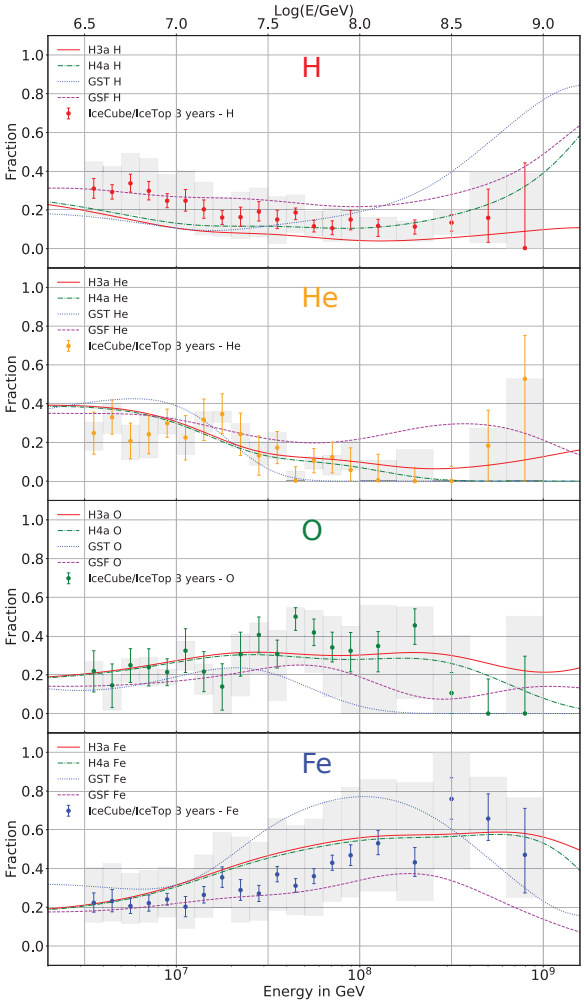

Figure 6: Fractions for the four elementary mass groups (H, He, O and Fe) [5] including the total detector systematic compared with various cosmic ray models (H3a and H4a [6]) and phenomenological experimental fits (GST [7] and GSF [8]). As a hadronic interaction model, Sibyll2.1 [4] is used in the simulated dataset.

energy output is a good estimator of the true energy, the mass output yields a broad distribution for a given element. Therefore, the composition can only be obtained statistically for the whole event sample by fitting distribution templates of four elementary mass groups (H, He, O and Fe) to the NN mass output[5]. In Figure 6, the mass composition fractions for these elementary groups as a function of the reconstructed energy are shown in comparison to CR propagation models. The elemental fraction results agree well with the prediction of the phenomenological models of the H3a and H4a [6] in this energy range. There are some clear differences in the shape of the fractions, especially the Fe fraction, in comparison to the prediction by the phenomenological data fits, Gaisser-Stanev-Tilav (GST) [7] fit and Global Spline Fit (GSF) [8]. However, inside the statistical and systematical uncertainties, none of these models can be ruled out. The calculated mean logarithmic mass $\langle \ln A \rangle$ also shows the predicted behavior of an increasingly heavier mass composition with increasing energies up to about 100–200 PeV, as shown in Figure 7. Given the statistical and systematic uncertainties, the reconstructed data beyond this point are consistent with either constant or decreasing mass composition. As shown in Figure 8, the absolute scale of the mass composition is dependent on the choice of the hadronic interaction model used for the simulations. The hadronic interaction model Epos-LHC [9] with a higher muon multiplicity leads to heavier mass composition measurements.

4 High-Energy Muon Multiplicity

Similar to the analysis in section 3, nearly vertical coincident events can be used to directly measure the TeV-muon multiplicity. This analysis [12] is based on a Neural Network (NN) reconstruction to simultaneously reconstruct

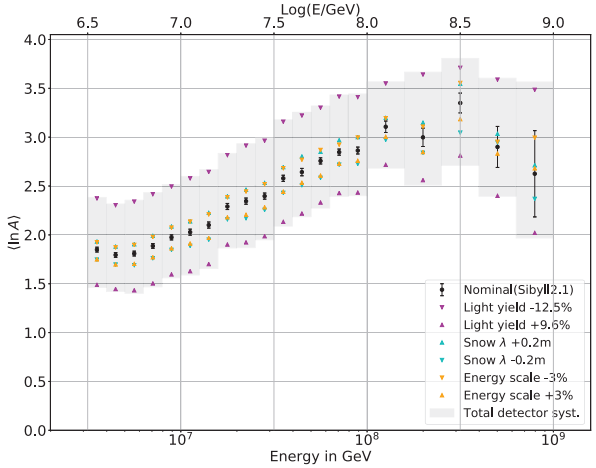

Figure 7: Calculated mean logarithmic mass $\langle \ln A \rangle$ with the total detector uncertainty(grey) from the combination of the light yield of the in-ice detector, snow correction and energy scale uncertainty [5].

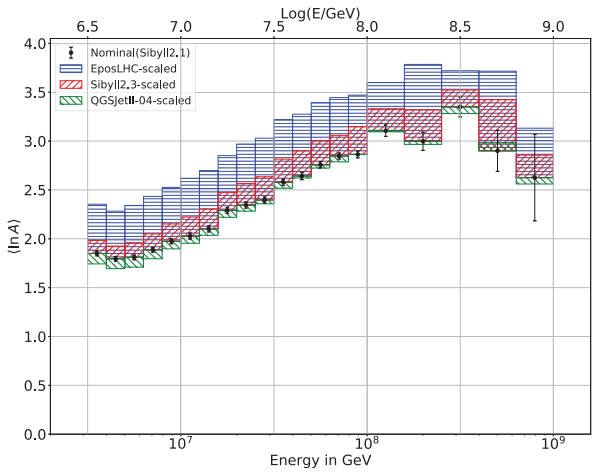

Figure 8: Hadronic interaction model uncertainty range on $\langle \ln A \rangle$ relative to the base model for Epos-LHC [9] (blue), Sibyll2.3 [10] (red) and QGSJetII-04 [11] (green) [5].

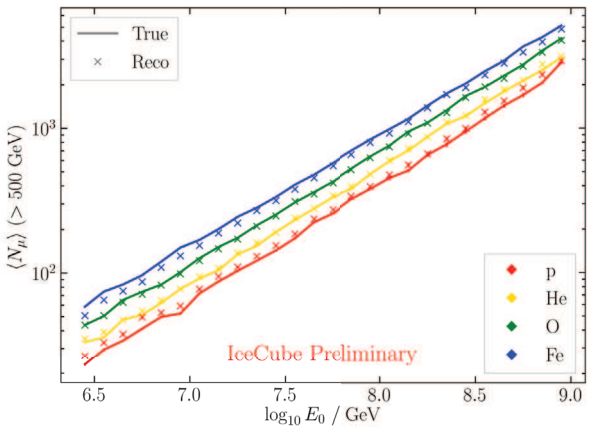

Figure 9: Average muon multiplicity $\langle N_\mu \rangle$ (> 500 GeV) as a function of primary energy in simulation obtained using the neural network determination of N_μ and E_0 compared to the true values for several elementary groups [12].

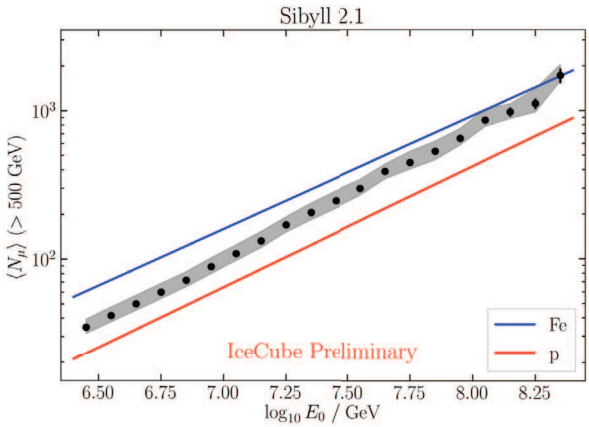

Figure 10: $\langle N_\mu \rangle$ with energy larger than 500 GeV as a function of primary energy [12], obtained from experimental data with Sibyll2.1 [4] simulation. Error bars indicate the statistical uncertainty and the band indicates the total systematic uncertainty.

the primary energy and the number of TeV-muons in the bundle. This NN uses inputs from IceTop, the shower size S_{125} (Eq. 1), the zenith angle, and from IceCube, the reconstructed energy loss profile. The full energy loss profile is transformed into a vector of 20 m segments for a recurrent neural network (RNN) layer. The combination of the RNN layer with the input variables from IceTop and several dense layers returns reconstructed values for E_0 and N_μ. For training, testing and validation, air shower simulations from 4 elementary groups (H, He. O and Fe) are used. The event-by-event neural network predictions are used to calculate the average multiplicity $\langle N_\mu \rangle$ per energy bin. As this reconstruction method shows a mass-dependent bias, dedicated simulation studies are used to derive correction factors, which are applied to compensate for neural network biases. In Figure 9, the reconstructed $\langle N_\mu \rangle$ is shown as a function of the primary energy E_0 for 4 elementary groups. This Figure demonstrates the small composition-depended biases of this method. A further simulation study is used to derive a correction for these biases [12]. The corrected experimental data are shown in Figure 10 in comparison to Sibyll2.1 simulations. For a better qualitative comparison, the measurements are re-scaled to the so-called "z-scale" [13]. In the "z-scale", the reconstructed muon number is normalized to the expected difference between the iron and proton simulation of a given hadronic interaction model. The re-scaling is defined as

$$z = \frac{\ln\langle N_\mu \rangle - \ln\langle N_\mu \rangle_p}{\ln\langle N_\mu \rangle_{Fe} - \ln\langle N_\mu \rangle_p}. \quad (2)$$

The re-scaling results for different hadronic interaction models are shown in Figure 11 in comparison to cosmic

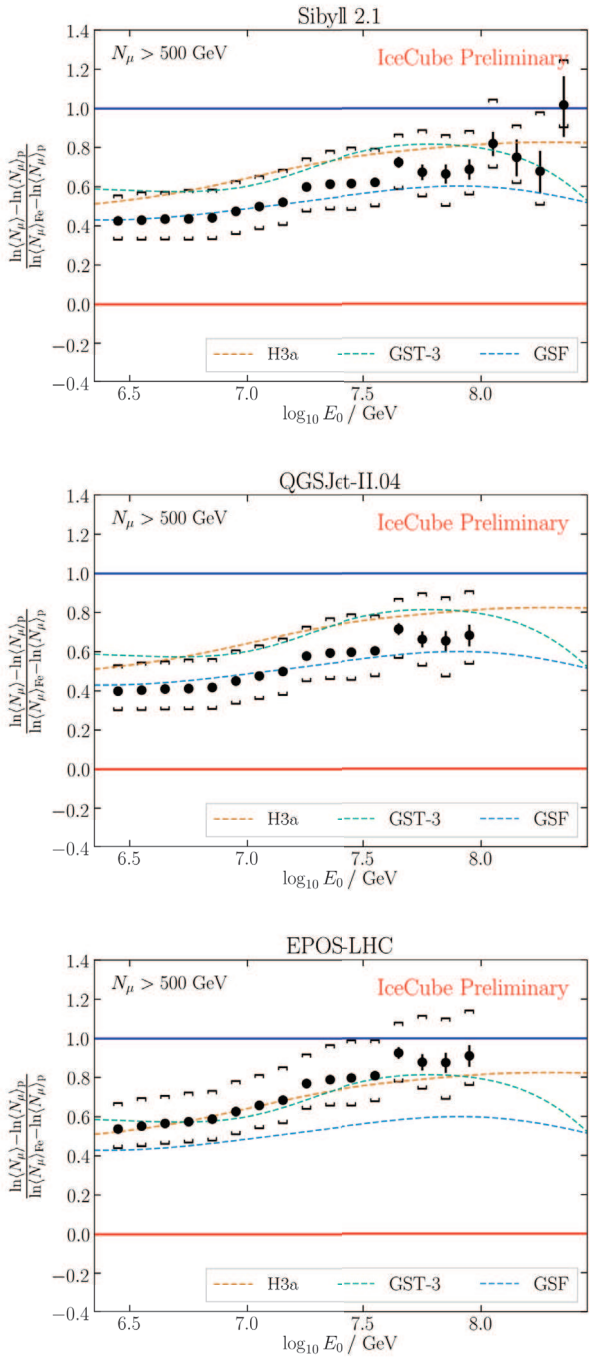

Figure 11: z-value results (Eq. 2) [12] with different hadronic interaction model assumptions, compared to expectations from mass composition models. Error bars indicate the statistical uncertainty and the brackets indicate the total systematic uncertainty.

ray models. Depending on the chosen hadronic interaction model some of the cosmic ray models describe the evolution of the data as a function of the reconstructed energy better than the other models. However, inside the statistical and systematical uncertainties, the results cannot rule out any of the expectations from the different mass composition models when assuming Sibyll 2.1 [4], QGSJet-II.04 [11] and EPOS-LHC [9] hadronic interaction models. Overall, these results show over the whole energy range the expected number of muons and do not see a muon deficit associated with other cosmic ray experiments[14].

5 IceTop - Surface Enhancement Detectors

Upgrades of the IceCube Neutrino Observatory are going to improve the mass composition sensitivity and reduce systematic uncertainties. The full surface array footprint of IceTop is currently been enhanced by additional surface stations, each consisting of 8 scintillator panels and 3 radio antennas [15]. A prototype of this new surface station is installed and taking successful data [16–18]. Additionally, 2 working prototypes of imaging air-Cherenkov telescopes IceAct [19–21] are installed at the South Pole.

5.1 IceTop Surface Enhancement

As the IceTop tanks get covered with additional snow every year, which is over time increasing the energy threshold, the surface scintillator panels are designed to mitigate the effect of snow attenuation as they are installed and kept above the snow level. A picture of a prototype scintillator panel at the South Pole is shown in Figure 12 (Top). These panels will also increase the sensitivity to study the surface muon density [22] of the air showers and add more observables for the study of the primary mass composition. The surface radio antennas are triggered by the scintillator stations. A picture of the radio antennas is shown in Figure 12 (Bottom left). These antennas will allow studying the air shower development of high-energy events inside the atmosphere, directly measuring the air shower maximum X_{max} for inclined air showers at the higher end of the observatories energy range. The preliminary results of a Monte Carlo study to estimate the X_{max} sensitivity are shown in Figure 13.

5.2 IceAct Telescopes

The IceAct telescopes are designed to withstand the environment of the South Pole, with a wide field of view of 12° to measure air showers inside the atmosphere at the lower end of the energy range from TeV to PeV. A picture of one of the IceAct prototypes is shown in Figure 12 (Bottom right). The measurement of air showers inside the atmosphere provides a complementary measurement to the surface array and in-ice response. This will allow independent reconstruction as well as improvement of the coincident analysis by providing additional detector observables. By using machine learning reconstruction, the air shower geometry, primary energy, and X_{max} can be measured simultaneously by using a single telescope. Improvements to this reconstruction are achieved by stereo observations by several telescopes or by hybrid measurement together with the other detector components. A preliminary graph neural network reconstruction using a single IceAct telescope [24] from the image for X_{max} is shown in Figure 14.

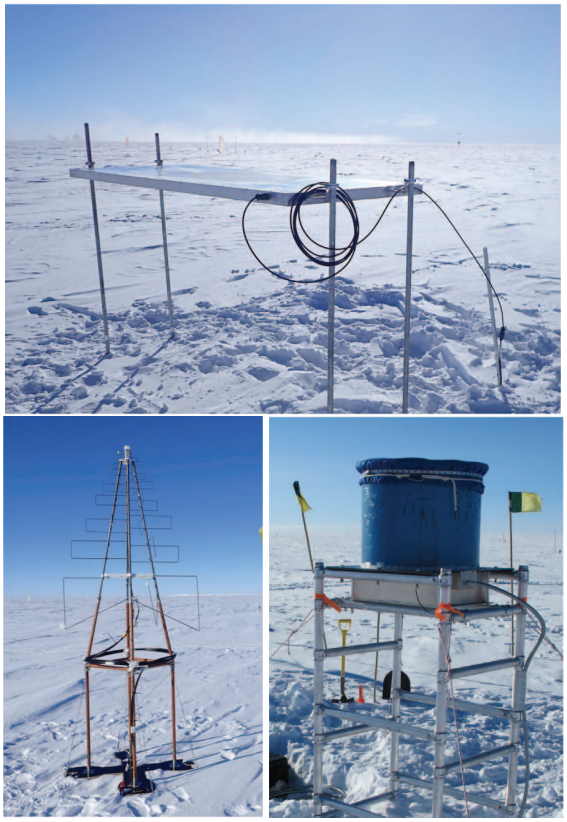

Figure 12: Surface enhancement prototype detectors - (Top) Surface scintillator panel [16–18], (Bottom left) Surface Radio antenna [17, 18] (Bottom right) Imaging air-Cherenkov telescope IceAct [19–21]. Pictures by Yuya Makino, IceCube/NSF

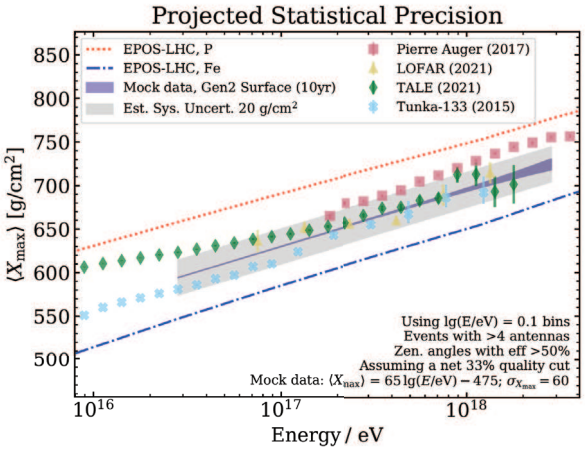

Figure 13: Projected precision from surface radio antennas for a measurement of X_{max} using 10 years of mock data and an IceCube-Gen2 detector [23].

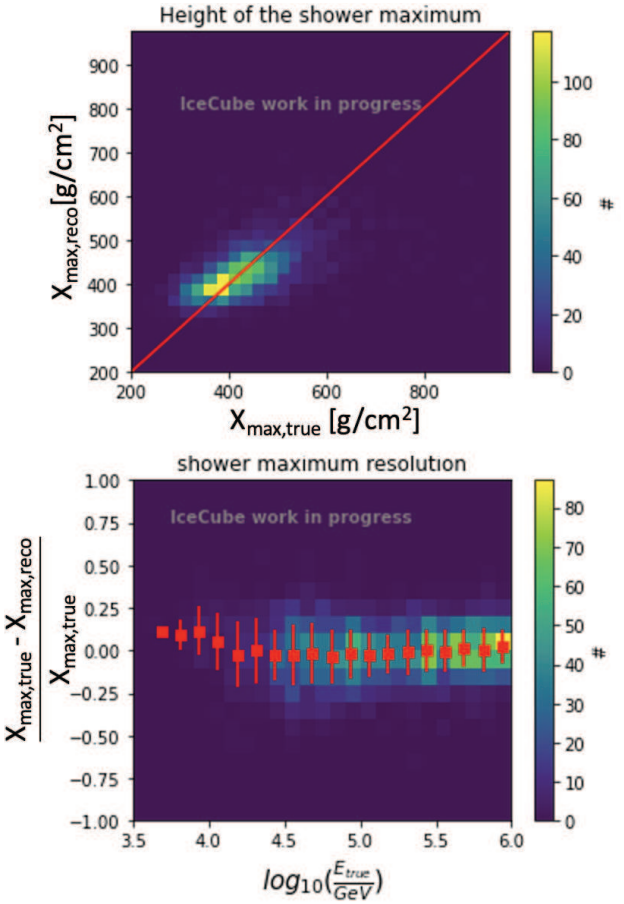

Figure 14: Preliminary IceAct graph neural network reconstruction result on the air shower maximum, trained with different elementary groups (H, He, N, Al and Fe) [24] using Sibyll2.1 [4] simulations. (Top) $X_{max,true}$ vs. $X_{max,reco.}$. (Bottom) Relative X_{max} resolution as a function of energy.

5.3 Future Outlook

In the near future, the IceCube Neutrino Observatory plans to upgrade the detector to instrumentalize an 8 times bigger volume with optical sensors and install a new shallow in-ice radio array to detect ultra-high energy (>100 PeV) neutrinos, called IceCube-Gen2 [25]. This new detector will also include an expanded surface array utilizing the already established new detector components, a scintillator panel array with radio antennas and a small IceAct telescope array. The schematic for this new detector layout and the IceTop surface enhancement is shown in Figure 15. With this larger detector, the upper energy bound for all analyses will be increased allowing cosmic ray studies to a few EeV with high enough statistics. With the increased number of surface/in-ice coincidences over a large energy range further tests of the hadronic interaction models can be performed to study the muon multiplicity. An improved in-ice detector component, a better in-situ calibration by new calibration devices, and new reconstruction techniques, like [26], will allow also provide a better mass

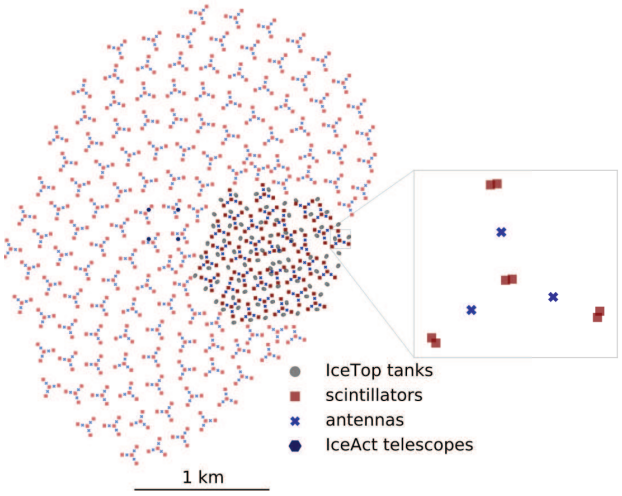

Figure 15: Layout of the currently under construction IceTop surface enhancement array (darker colors) and the proposed surface component of the future IceCube-Gen2. Modified from [23].

composition resolution and smaller systematic uncertainties.

6 Summary

The analyses presented here show the scientific capabilities of the IceCube Neutrino Observatory as a unique cosmic ray detector for mass composition in the energy range from PeV to EeV. The evolution of the mass composition fractions as a function of energy from the elementary groups as well as the measurements of TeV-muon multiplicities show reasonable agreement between the data from IceCube and IceTop and the prediction from cosmic ray models in this energy range. However, the measurements cannot discriminate any models yet. In the near future, these results will be improved by the addition of new detector components. The planned IceCube-Gen2 will further enhance the measurements of the primary cosmic ray mass composition by the increased detector size and improved new detector components.

References

[1] M.G. Aartsen et al. (IceCube), JINST **12**, P03012 (2017)
[2] S. Verpoest, D. Soldin, S. De Ridder (IceCube), PoS **ICRC2021**, 357 (2021)
[3] R. Abbasi et al. (IceCube), Nucl. Instr. and Meth. A **700**, 188 (2013)
[4] E. Ahn, R. Engel, T. Gaisser, P. Lipari, T. Stanev, Physical Review D **80**, 94003 (2009)
[5] M.G. Aartsen et al. (IceCube), Phys. Rev. D **100**, 082002 (2019)
[6] T.K. Gaisser, Astroparticle Physics **35**, 801 (2012)
[7] T.K. Gaisser, T. Stanev, S. Tilav, Front. Phys. (Beijing) **8**, 748 (2013)
[8] H.P. Dembinski, R. Engel, A. Fedynitch, T. Gaisser, F. Riehn, T. Stanev, PoS **ICRC2017**, 533 (2018)
[9] T. Pierog, I. Karpenko, J.M. Katzy, E. Yatsenko, K. Werner, Phys. Rev. C **92**, 034906 (2015)
[10] F. Riehn, R. Engel, A. Fedynitch, T.K. Gaisser, T. Stanev, PoS **ICRC2015**, 558 (2016)
[11] N.N. Kalmykov, S.S. Ostapchenko, A. Pavlov, Nucl. Phys. B Proc. Suppl. **52** (1997)
[12] S. Verpoest (IceCube), PoS **27th European Cosmic Ray Symposium**, 074 (2022)
[13] H.P. Dembinski et al., EPJ Web Conf. **210**, 02004 (2019)
[14] J. Albrecht et al., Astrophys. Space Sci. **367**, 27 (2022)
[15] A. Haungs (IceCube), EPJ Web Conf. **210**, 06009 (2019)
[16] M. Kauer, T. Huber, D. Tosi, C. Wendt (IceCube), PoS **ICRC2019**, 309 (2019)
[17] M. Oehler, R. Turcotte (IceCube), PoS **ICRC2021**, 225 (2021)
[18] A. Coleman, H. Dujmovic, M. Oehler (IceCube), PoS **ICRC2021**, 314 (2021)
[19] M. Aartsen, et al. (IceCube), JINST **15**, T02002–T02002 (2020)
[20] K. Andeen, M. Schaufel, J. Auffenberg (IceCube), PoS **ICRC2019**, 179 (2019)
[21] L. Paul, M. Schaufel, M. Plum (IceCube), PoS **ICRC2021**, 276 (2021)
[22] R. Abbasi et al. (IceCube), Phys. Rev. D **106**, 032010 (2022)
[23] A. Coleman et al., Astropart. Phys. **147**, 102794 (2023)
[24] L. Paul, T. Bretz, J. Hewitt, A. Zink (IceCube) (2022), `https://doi.org/10.5281/zenodo.6354743`
[25] M.G. Aartsen et al. (IceCube-Gen2), J. Phys. G **48**, 060501 (2021)
[26] P. Koundal (IceCube), PoS **27th European Cosmic Ray Symposium**, 085 (2022)